Stability of equidimensional pseudo-single-domain magnetite over billion-year timescales

Stability of Equidimensional Pseudo-Single Domain Magnetite Over Billion Year Time-Scales

Lesleis Nagy[a,1], **Wyn Williams**[a], **Adrian R. Muxworthy**[b], **Karl Fabian**[c], **Trevor P. Almeida**[d], **Pádraig Ó Conbhuí**[a], **and Valera P. Shcherbakov**[e,f]

[a]School of Geosciences, University of Edinburgh, The King's Buildings, James Hutton Road, Edinburgh, EH9 3FE, UK; [b]Department of Earth Science and Engineering, Imperial College London, South Kensington Campus, London, SW7 2AZ, UK; [c]Norges Geologiske Undersøkelse, Leiv Eirikssons vei 39, 7040 Trondheim, Norway; [d]School of Physics and Astronomy, University of Glasgow, Glasgow, G12 8QQ, UK; [e]Geophysical Observatory of Russian Academy of Sciences, Borok, Yaroslvaskaya oblast, 152742, Russia; [f]Institute of Physics of the Earth of RAS, Moscow, Institute of Geology and Petroleum Technologies, Kazan Federal University, Russia

This manuscript was compiled on August 9, 2017

Interpretations of paleomagnetic observations assume that naturally occurring magnetic particles can retain their primary magnetic recording over billions of years. The ability to retain a magnetic recording is inferred from laboratory measurements, where heating causes demagnetization on the order of seconds. The theoretical basis for this inference comes from previous models that assume only the existence of small, uniformly magnetized particles, whereas the carriers of paleomagnetic signals in rocks are usually larger, non-uniformly magnetized particles, for which there is no empirically complete, thermally-activated model. This study has developed a thermally-activated numerical micromagnetic model that can quantitatively determine the energy barriers between stable states in non-uniform magnetic particles on geological time scales. We examine in detail the thermal stability characteristics of equidimensional cuboctahedral magnetite and find that contrary to previously published theories, such non-uniformly magnetized particles provide greater magnetic stability than their uniformly magnetized counterparts. Hence, non-uniformly magnetized grains, which are commonly the main remanence carrier in meteorites and rocks, can record and retain high-fidelity magnetic recordings over billions of years.

micromagnetics | paleomagnetism | geomagnetism

Since the 1900s magnetic recordings observed in rocks and meteorites have been studied to understand the evolution of the Earth and the Solar System. The validity of the findings from these studies depends on a theoretical understanding of rock-magnetic recordings provided by Néel (1, 2) and numerous experimental studies, for example, Strangway et. al. (3) and Evans and Wayman (4). The overwhelming evidence from these authors was that stable natural magnetic remanence (NRM) in rocks resides within ultrafine, uniformly magnetized particles, called single domain (SD) particles. Néel's theory (1, 2) for the behavior of thermally-activated SD particles describes a unique relationship between thermal and temporal stability and gave confidence that paleomagnetic recordings that become unstable (unblocked) only at high temperatures, retain magnetic recordings from the time of their mineral crystallization, possibly as far back in time as four billion years ago.

However, in the 1970s and 80s the widespread use of hysteresis parameters to characterize magnetic mineralogy (5) found that the majority of magnetic particles in rocks are not in uniform magnetic states, but are larger in size (80 – 1000 nm) and contain complex magnetic states that are not described by either SD theory or the multidomain (MD) theory of micron-sized particles (2, 6). The term pseudo-single-domain (PSD) was coined for such particles and much effort was spent in determining the origin of their magnetic fidelity (7, 8). Due to the complexity of the problem it has not been possible to determine the temporal stability of magnetisation in PSD grains on geological time scales from their observed thermal stability in the laboratory, although this stability is usually assumed (9, 10). It was therefore difficult to claim with any degree of certainty that the measured paleomagnetic signal of most rocks and meteorites containing PSD grains represents the magnetic field recorded when the mineral formed.

We consider here only the simplest form of PSD grains, which are single vortex (SV) magnetic domain states that form in equidimensional magnetite grains from 80 nm to 1000 nm. Beyond this grain size more complex non-uniform PSD states will exist that may consist of multiple vortices or MD regions with broad domain wall-like structures.

We have introduced the nudged-elastic-band (NEB) method, which minimizes the action along the energy path (11–14) into a finite element method (FEM) micromagnetic model to determine the energy barriers between possible magnetic states as a function of temperature. We used the NEB algorithm to determine the thermal behavior, the temperature of magnetic stability (blocking temperature) and relaxation times for equidimensional SD and SV grains of magnetite. This study finds that magnetically non-uniform SV magnetite particles that are ubiquitous in nature, have high blocking temperatures close to their Curie temperature and long relaxation times, and as such offer a much higher magnetic recording

Significance Statement

When magnetic crystals form in rocks and meteorites, they can record the ancient magnetic field, and retain this information over geological time-scales. Scientists use these magnetic recordings to study the evolution of the Earth and Solar System. Previous theories for the recording mechanisms of the magnetic crystals in rocks and meteorites are based on the idea that the magnetic structures within crystals are near uniform. However, from numerous studies we know this not to be true. The crystals are too large in size and display complex non-uniform 'vortex' structures. In this study we have shown for the first time that vortex structures are capable of recording and retaining magnetic signals over billions of years.

L.N. and W.W. designed research; L.N. performed research; L.N., W.W. and A.R.M. performed data analysis; and L.N., W.W., A.R.M., K.F., T.P.A., P.Ó.C and V.P.S. wrote the paper.

The authors declare no conflict of interest.

[1]To whom correspondence should be addressed. E-mail: l.nagyed.ac.uk

fidelity than equidimensional SD particles.

To determine the thermally-activated stability of magnetite particles, all possible local-energy minimum (LEM) states for particles with a given volume at a given temperature need to be found. This was achieved by initializing the geometry with random magnetisation directions and minimizing the free energy with respect to temperature dependent values for the saturation magnetisation, magnetocrystalline anisotropy and exchange constant (15–17) (see materials and methods). Although no computational method can guarantee that all possible LEM states have been found, after executing several thousands of simulations, the only domain states seen to nucleate were the ones described below. For example, in a cuboctahedral particle equivalent to a spherical volume with 100 nm diameter (abbreviated to ESVD), at 20°C, we identified 16 LEM states corresponding to SV structures with vortex cores directed along one of four cubic diagonals, which are the magnetocrystalline easy axes in magnetite. Figure 1 identifies eight such structures for a right-handed vortex, there are a further eight for a left-handed vortex with equal preference for both left- and right-handed structures.

The NEB method (11–14) was used to calculate the energy barriers between two LEM states by determining the most energetically favourable path between those two states. We found it unnecessary to compute energy barriers across all possible (120) pairs of LEM states, because many energy paths and barriers are equivalent (Fig. 1). For example, equivalent paths were identified for the 100 nm (ESVD) cuboctahedron at 20°C by calculating and directly comparing energy paths for all possible permutations of start/end pairs; the summary of these results is shown in Figure 2 and indicates two fundamental classes of transition: same-sense reorientations, where the handedness of the vortex-core does not change; and vortex-core unwindings, where the vortex-core switches from clockwise to anti-clockwise or *vice versa*.

We identified two types of same-sense vortex-core reorientations: (i) small-angle reorientations, and (ii) large-angle reorientations. Small-angle reorientations of the vortex core represent a rotation of approximately 71°, corresponding to the angle between two of the nearest-neighbour cubic diagonals. In this transition, the vortex core remains right- or left-handed, and the energy graph illustrates a single smooth peak (Fig. 2a) corresponding to a single energy barrier between start and end states. Large-angle reorientations are vortex-core transitions through angles greater than 71°. The energy graph for a large-angle transition illustrates a smooth initial path, corresponding to a 71° reorientation, and a second, noisier section (Fig. 2b). This noisy section reflects the fact that the NEB method we used only guarantees the resolution of a single energy barrier between any two LEM states; the second transition is therefore not effectively resolved. However, the full transition can be determined by breaking the path into several shorter sections, and individually determining the barriers along each section. Consequently, large-angle transitions are simply resolved as chains of small-angle transitions. When we consider transition paths with a change of vortex-core orientation from a left-handed sense to a right-handed sense (Fig. 2c). An initial large energy peak is seen, followed by three much smaller peaks each of the same maximum energy as a small-angle reorientation, as seen in Figure 2a. This behaviour corresponds to an initial high-energy unwinding of the vortex core propagating from one end of the vortex to the other, followed by a vortex-core rotation through 180° via three successive small-angle rotations (supplementary animations S1 – S3).

Through exploration of the energy paths of each transition pair we reduced the number of NEB calculations for each cuboctahedral geometry from potentially 120 pairs down to one, greatly simplifying the problem of mapping out relaxation times for a range of temperatures and grain sizes. This was possible because all the unwinding-class transitions were discounted as being energetically unlikely, and transitions between same-handed structures are energetically equivalent to a single small-angle rotation.

To determine thermal stability, we then calculated energy barriers as a function of temperature for equidimensional truncated cuboctahedral magnetite particles (Fig. 1), with sizes from 40 nm to 170 nm (ESVD) increasing in steps of at most 10 nm. The temperature range for NEB calculations was 20°C to 550°C increasing in steps of 10°C.

In Figure 3 we summarize this study's results for the blocking temperatures of equidimensional magnetite particles from the SD size up to well above the SD/SV transition size (∼80 nm), and compare them to analytical SD theory (2) (the graph for SD grains is extended beyond the usual SD range for magnetite for comparison). There are some very clear trends. Cuboctahedral magnetite particles in the SD range - smaller than ∼70 nm are thermally unstable and have blocking temperatures below 100°C, in agreement with analytical SD theory. Beyond ∼70 nm significant departure from analytic theory is found with higher blocking temperatures predicted to just over 200°C at ∼80 nm. Blocking temperature then decreases after ∼84 nm until ∼100 nm. This divergence is because micromagnetic models for SD particles allow for departures from the perfect magnetic uniformity assumed in Néel's theory. For example, larger SD particles display so-called 'flowering' at particle edges (18), which increases energy barriers and in turn blocking temperatures as the particle size approaches the SD-SV threshold size (Fig. 3). The unstable zone observed between ∼84 nm to ∼100 nm is due to a switching mechanism different to most of the particles in this study since they result from switching between, hard-axis-aligned vortices. From ∼100 nm onwards, the most energetically stable structures are observed to be distinct, easy-axis-aligned vortex cores.

For SV magnetite (with easy-aligned vortex-cores), the blocking temperature increases with particle size from less than 100°C for particles at ∼100 nm, up to temperatures close to the Curie temperature (∼580°C) of magnetite for particles greater than 150 nm ESVD. The reason for these high blocking temperatures is clear when we examine the switching mechanisms in single vortex-core models (supplementary animations S1 - S3). When the vortex state traverses along the minimum energy path, we see a 'structure-coherent rotation'(SCR) of the vortex-core from one easy axis to the next. This is not coherent rotation as observed in SD grains where each component of the magnetisation rotates by the same amount throughout the grain, instead the whole vortex structure rotates, and in so doing, retains its vortex character throughout the transition. This is most clearly seen in the supplementary movies (S1 - S3). Thus, we may think of the switching between minimum energy states in SV grains as a rotation of the vortex core, analogous to coherent switching of uniform magnetisation in

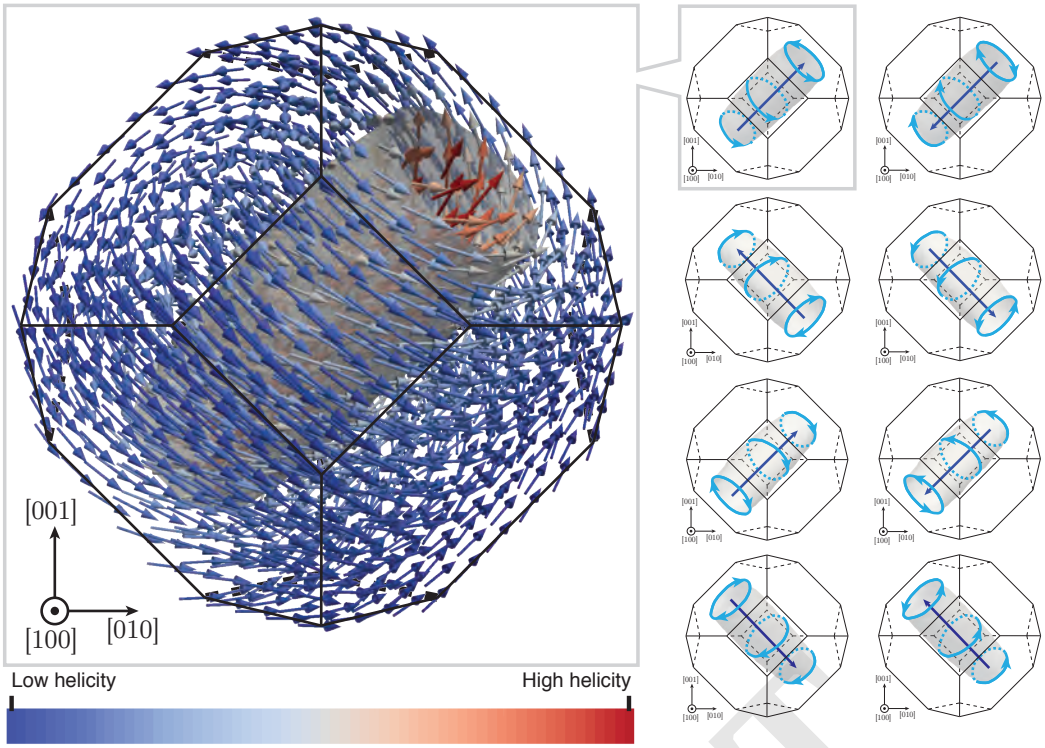

Fig. 1. A typical single vortex state in an equidimensional cuboctahedral grain of magnetite equivalent to a spherical volume diameter (ESVD) of 100 nm. This grain is coloured by the helicity, defined as the amount of local twisting of the magnetisation field (negative values correspond to left hand sense twisting and positive values correspond to right hand sense). Schematics for the eight possible orientations of the vortex core with respect to a right-handed sense are illustrated on the right (the top left schematic corresponds to the magnetic structure shown). There are an additional eight structures with a left-handed sense twisting. The thermal stability of the grain depends upon the energy barriers between any two possible LEM states. The symmetry in the domains states seen on the right allow us to greatly reduce the number energy barrier calculations required to determine its thermal stability.

SD particles (19). This increase in blocking temperature with increasing vortex-core particle size has recently been hinted at experimentally (20), but has not, until now, been explained by either analytical or numerical models.

It is interesting to compare the SD and SV calculated blocking temperatures shown in Figure 3. For cuboctahedral magnetite, the calculations predict that SV particles have higher blocking temperatures than SD particles, in contrast to previous models (2, 6, 21) for non-uniform magnetisation structures, which predict the opposite trend. As the effective volumes associated with SCR are larger than in coherent SD switching, this increases the blocking temperatures to close to the Curie temperature and explains the experimental observation of high palaeomagnetic stability (Fig. 3).

To determine the magnetic stability of magnetic remanence at room temperature, we use equation 5 (see materials and methods) and a temperature of 20°C to determine relaxation times as a function of particle size (Fig. 3). For small (SD) particles, the stability peaks at ∼80 nm with a relaxation time greater than the age of the universe. For particles smaller than 70 nm, the calculations of this study agree well with analytical SD theory (2) (Fig. 3) However, for particles larger than 70 nm there is strong divergence in predicted relaxation times (Fig. 3). Again, as described above, this divergence is due to flowering of magnetic structures in larger SD particles in the micromagnetic models.

For single vortex-core cuboctahedrons just above the SD-SV transition size, the relaxation time is less than 60 s, but increases sharply to greater than the age of the universe by 100 nm, and continues to increase for all the particle sizes up to the maximum size of 170 nm considered in this study.

In comparison with SD particles, equidimensional magnetite with SV magnetisation structures have longer relaxation times, and hence greater stability than equidimensional SD grains. It is important to note of course, that shape elongation of small SD particles will greatly enhance their magnetic stability and so SD grains will remain an ideal domain state for paleomagnetic recording. However, here we have shown that grains containing SV domain states, which in many rock samples may constitute the majority, are still able to hold a paleomagnetic recording with a high thermal stability and have relaxations times at room temperature that exceed the age of the universe. Although single vortex domain states have been identified theoretically (22) and experimentally (23) for some years, we believe that the results of the present study is the first indication that these domains states have sufficient thermal and temporal stability to make them excellent carriers of paleomagnetic information. Indeed the high blocking temperatures of SV particles predicted by this model are supported by recent high-temperature nanometer scale magnetic imaging (20, 24–26) of SV magnetite particles.

By examining switching mechanisms in idealized magnetic grains, we can finally explain an observation central to paleomagnetism: the apparent contradiction between the recording stability and fidelity of natural magnetic systems that also display magnetic-hysteresis characteristics of particles with non-

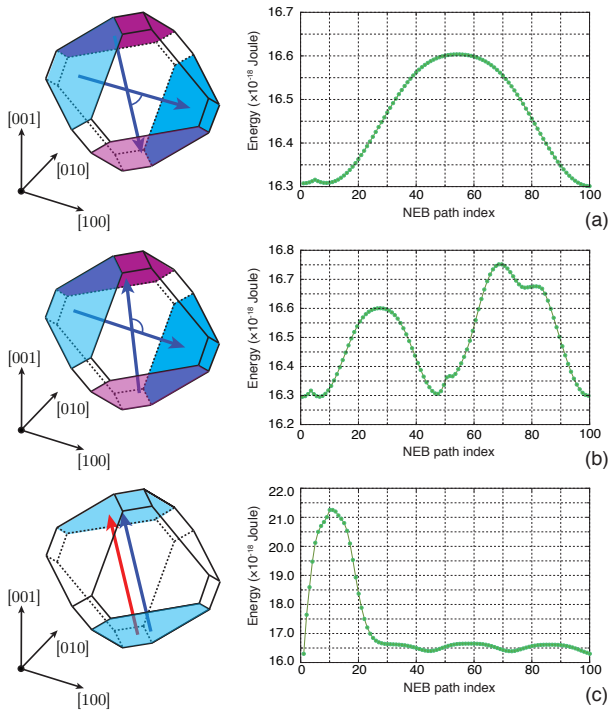

Fig. 2. Three fundamental types of transition. The left schematics show the type of transition (with blue arrows corresponding to right-handed vortex core orientations and red arrows corresponding to left-handed vortex core orientations). The blue and purple areas indicate the start and end of vortex cores on the surface of the grain. The graphs to the right of the schematics illustrate the energies along the path between the two endpoints – each point on of the graph is a separate magnetisation structure.

uniform magnetic structures, which until now were assumed to indicate poor magnetic recording fidelity. By demonstrating that SV magnetite particles are of high magnetic stability, we have shown that there is no inconsistency. Whilst it is undoubtedly true that PSD grains with more complex domains states will contribute to the magnetic remanence, SV states will be some of the highest PSD remanence carriers whilst also accounting for a large grain size range (∼80 – ∼1000 nm compared to ∼50 – ∼80 nm for SD grains (27)). The findings are also not just limited to magnetite, which we have focused on in this study due to its ubiquity in nature and importance to paleomagnetism and its applications. The findings will also be applicable to other magnetic systems that display SV structures, *e.g.*, greigite (28) found in sediments and metallic iron (29) found in meteorites.

Materials and Methods

Magnetisation structures in particles are classified into three basic types: (i) SD, where all magnetisation vectors are oriented in the same direction; (ii) PSD, where vectors are arranged into inhomogeneous structures, but are not able to form well-defined domains; and (iii) MD, which contain distinct uniformly magnetised regions separated by domain walls. In this study, calculation of SV states (being the simplest of PSD states) were made using FEM micromagnetic algorithms (18, 30) this technique allows accurate modelling of geologically realistic magnetic particles by taking a geometric description of a magnetic particle and dividing it into many small tetrahedral segments. The magnetic free energy is then calculated for each segment and the total free energy is the discrete sum over all tetrahedra. The FEM method discretizes the total free energy $E_{\rm tot}$, for some configuration of magnetisation m in a magnetic grain, given by (31)

$$E_{\rm tot} = \int_{\Omega} \left[A\,|\nabla \vec{m}|^2 + K_1 \left(m_x^2 m_y^2 + m_x^2 m_z^2 + m_y^2 m_z^2 \right) - M_{\rm s} \left(\vec{H}_{\rm z} \cdot \vec{m} \right) - \frac{1}{2} \left(\vec{H}_{\rm d} \cdot \vec{m} \right) \right] d\Omega, \quad [1]$$

where the temperature-dependent material parameters are denoted by A for the exchange constant; K_1 for magneto-crystalline anisotropy; and $M_{\rm s}$ for saturation magnetisation and are taken from (15–17). The externally-applied field is denoted by $H_{\rm z}$ and the self-demagnetising field is $H_{\rm d}$.

The temperature dependent material parameters for equation 1 are given by experimentally derived expressions (16, 17, 32) and have the following forms

$$A = \frac{\sqrt{2.16225 \times 10^4 + 816.476(T_{\rm C} - T)} - 147.046}{4.08238 \times 10^{13}} \quad [2]$$

$$M_{\rm s} = 3.82525 \times 10^4 (T_{\rm C} - T)^{0.4} \quad [3]$$

$$K_1 = -2.13074 \times 10^{-5} (T_{\rm C} - T)^{3.2} \quad [4]$$

where $T_{\rm C} = 580°$C is the Curie temperature of magnetite.

To determine the thermal stability of a particle, it is necessary to find the energy barriers that exist between all possible stable domain states at all possible temperatures within a sample; energetically stable configurations correspond to magnetisation states where the free energy, $E_{\rm tot}$, is minimised. In this study, the LEM states were found using a modified-conjugate gradient method (11, 14).

Once two suitable start and end points are selected, the NEB method is used to compute an energy barrier. Figure 4 illustrates the NEB concept in terms of the well-documented case of a uniformly magnetised ellipsoid (19). Path start and end points correspond to magnetisations aligned along the [100] axis (with $\theta = 0$ and $\phi = \pi/2$) on the left and [$\bar{1}$00] (with $\theta = \pi$ and $\phi = \pi/2$) on the right. The NEB method first selects an initial path (illustrated by the red line in Fig. 4), which is then evolved along the energy surface to minimise the total action (11–14) along the path. The final energy path represents the most favourable transition between start and end points (illustrated by the white line in Fig. 4), and it can be seen to pass through the magnetisation in the direction (with $\theta = \pi/2$ and $\phi = \pi/4$) which is the theoretical energy maximum along the path, as expected (19).

To calculate the blocking temperature, $T_{\rm B}$, for a particle of magnetite, for a given relaxation time τ, we use the Néel-Arrhenius (2) relation

$$\tau = \frac{1}{C} \exp\left(\frac{\Delta E}{k_{\rm B} T} \right) \quad [5]$$

where C is the atomic switching frequency (taken to be 10^{-9} s), $k_{\rm B}$ is Boltzmann's constant, T is the temperature in degrees Kelvin and ΔE is the energy barrier between LEM states, which we calculate in this study using the NEB method. To calculate blocking temperatures for SV particles, we determined ΔE for each size and temperature. The relaxation times were then calculated for a range of temperatures using NEB derived values of ΔE and equation 5. A polynomial fit was then made of the calculated relaxation times in order to determine the blocking temperature – a reference time of 100 seconds was chosen since it is on the order of the time used in laboratory experiments (33). This time point indicated by the dashed red line in Figure 5.

All models shown in this paper were produced using the Micromagnetic Earth Related Robust Interpreter Language Laboratory (MERRILL), the source code of which is publicly available at `https://bitbucket.org/wynwilliams/merrill`.

ACKNOWLEDGMENTS. This work is supported by the Natural Environment Research Council (grant NE/J020966/1) and European Research Council (grant EC320832 IMAGINE). We would also like to thank the reviewers for their helpful suggestions.

1. Néel L (1955) Some theoretical aspects of rock-magnetism. *Advances in physics* 4(14):191–243.
2. Néel L (1949) Théorie du traniage magnétique des ferromagnétiques en grains fines avec applications aux terres cuites. *Annales Geophysicae* 5:99–136.

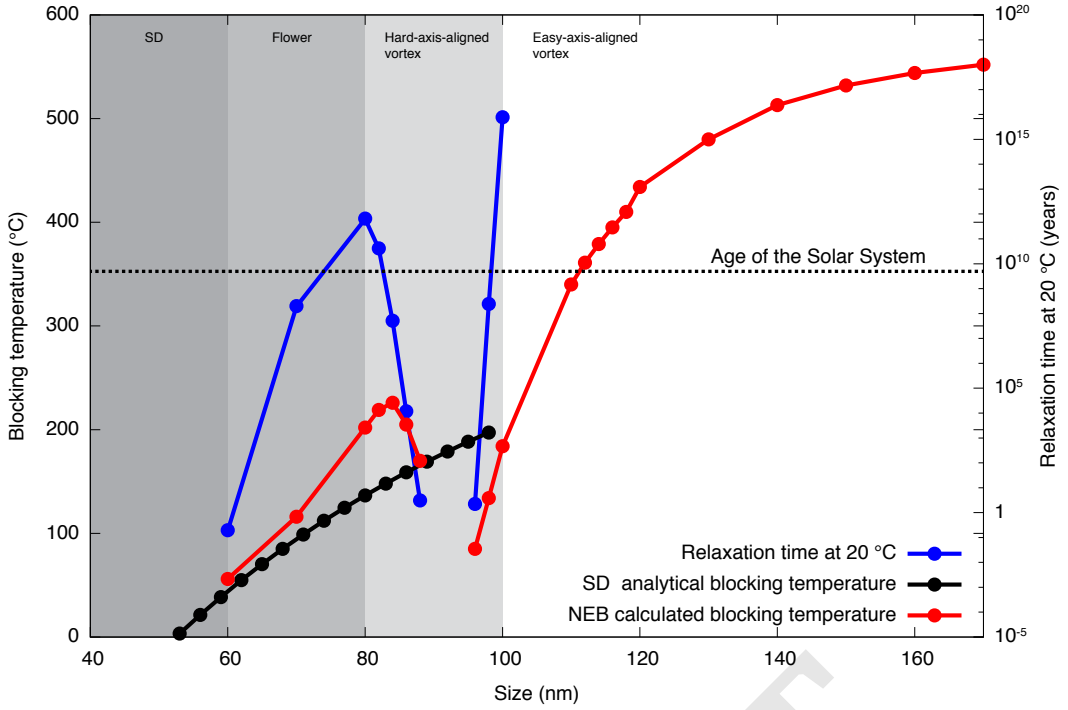

Fig. 3. Blocking temperatures for equidimensional cuboctahedral magnetite. The red line shows the blocking temperatures calculated using the NEB in our study. We assume that grains are unblocked if their relaxation time falls below 100 seconds. There is an increase in thermal stability as the grain evolves from SD, in the 40 nm – 60 nm equivalent spherical volume diameter (ESVD) range, to flower from 60 nm – 70 nm (ESVD). The black line shows blocking temperatures calculated from SD theory, illustrating how the predicted blocking temperatures in our model diverge from the SD values due to flowering. From 80 nm – 94 nm (ESVD) the LEM states are observed to be hard-axis-aligned vortices and from 96 nm onwards we see vortex states. The blue line illustrates the room temperature relaxation time for our grain.

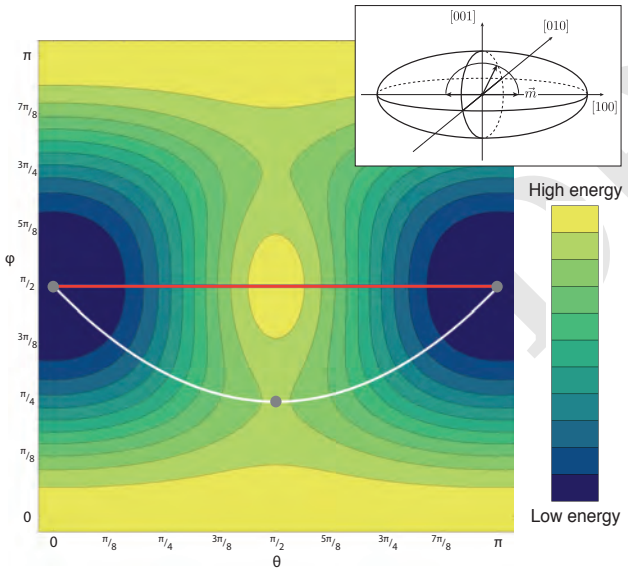

Fig. 4. Minimum energy path for a uniformly magnetised prolate ellipsoid (inset). The variables θ and ϕ represent the magnetisation direction in spherical coordinates and the contours represent the magnetic energy in the absence of an externally applied field. Light colours represent configurations of high energy (corresponding to anisotropic hard axes) and dark colours low energy (anisotropic easy axes). An initial path (shown in red) is evolved to the path of least action (shown in white) by the NEB.

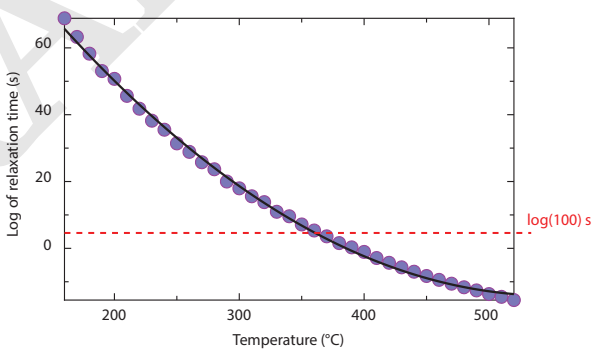

Fig. 5. Evaluation of blocking temperature for a given relaxation time (indicated by the dotted line). Given a set of relaxation times near the blocking temperature, a polynomial line is fitted. This line may then be used to select the blocking temperature at the precise reference time (in this case 100 s).

3. Strangway DW, Larson EE, Goldstein M (1968) A possible cause of high magnetic stability in volcanic rocks. *Journal of Geophysical Research* 73(1):3787–3795.
4. Evans ME, Wayman ML (1970) An investigation of small magnetic particles by means of electron microscopy. *Earth and Planetary Science Letters* 9(4):365–370.
5. Day R (1977) TRM and its variation with grain size. *Journal of Geomagnetism and Geoelectricity* 29:233–265.
6. Dunlop DJ, Xu S (1994) Theory of partial thermoremanent magnetization in multidomain grains. 1: Repeated identical barriers to wall motion (single microcoercivity). *Journal of Geophysical Research* 99(B5):9005–9023.
7. Dunlop DJ (1977) The hunting of the 'psark'. *Journal of Geomagnetism and Geoelectricity* 29:293–318.
8. Moon TS, Merrill RT (1985) Nucleation theory and domain states in multidomain magnetic material. *Physics of the Earth and Planetary Interiors* 37:214–222.
9. Tarduno JA, Cottrell RD, Davis WJ, Nimmo F, Bono RK (2015) A Hadean to Paleoarchean geodynamo recorded by single zircon crystals. *Science* 349(6):521–524.
10. Cournede C, et al. (2015) An early solar system magnetic field recorded in CM chondrites. *Earth and Planetary Science Letters* 410:62–74.
11. Fabian K, Shcherbakov VP (2017) The physics of viscous magnetization in multidomain particles: energy barriers in three-dimensional micromagnetic models. *Journal of Magnetism and*

Magnetic Materials.
12. Dittrich R, et al. (2002) A path method for finding energy barriers and minimum energy paths in complex micromagnetic systems. *Journal of Magnetism and Magnetic Materials* 250.
13. Henkelman G, Uberuaga BP, Jónsson H (2000) A climbing image nudged elastic band method for finding saddle points and minimum energy paths. *Journal of Chemical Physics* 113(22):9901–9904.
14. Berkov DV (1998) Numerical calculation of the energy barrier distribution in disordered many-particle systems: the path integral method. *Journal of Magnetism and Magnetic Materials* 186(1):199–213.
15. Pauthenet R (1952) Aimantation spontanée des ferrites. 7:710–747.
16. Heider F, Williams W (1988) Note on temperature dependence of exchange constant in magnetite. *Geophysical Research Letters* 15(2):184–187.
17. Fletcher EJ, O'Reilly W (1974) Contribution of Fe2+ ions to the magnetocrystalline anisotropy constant K1 of Fe3-xTixO4 (0<x<0.1). *Journal of Physics C: Solid State Physics* 7(1):171–178.
18. Williams W, Dunlop DJ (1989) Three-dimensional micromagnetic modelling of ferromagnetic domain structure. *Nature* 337(6):634–637.
19. Stoner EC, Wohlfarth EP (1948) A mechanism of magnetic hysteresis in heterogeneous alloys. *Philosophical Transactions of the Royal Society of London, Series A: Mathematical, Physical and Engineering Sciences* 240:599–642.
20. Almeida TP, et al. (2016) Direct observation of the thermal demagnetization of magnetic vortex structures in nonideal magnetite recorders. *Geophysical Research Letters* 43(1):8426–8434.
21. Shcherbakov VP, McClelland E, Shcherbakova VV (1993) A model of multidomain thermoremanent magnetization incorporating temperature-variable domain structure. *Journal of Geophysical Research* 98(B4):6201–6216.
22. Schabes ME, Bertram HN (1988) Magnetization processes in ferromagnetic cubes. *Journal of Applied Physics* 64(3):1347–1357.
23. Shinjo T, Okuno T, Hassdorf R, Shigeto K, Ono T (2000) Magnetic Vortex Core Observation in Circular Dots of Permalloy. *Science* 289(5481):930–932.
24. Almeida TP, et al. (2014) Observing thermomagnetic stability of nonideal magnetite particles: Good paleomagnetic recorders? *Geophysical Research Letters* 41(20):7041–7047.
25. Almeida TP, et al. (2014) Visualized effect of oxidation on magnetic recording fidelity in pseudo-single-domain magnetite particles. *Nature Communications* 5:5154.
26. Almeida TP, et al. (2016) Direct visualization of the thermomagnetic behavior of pseudo-single-domain magnetite particles. *Science Advances* 2(4):e1501801–e1501801.
27. Dunlop DJ (1973) Superparamagnetic and single-domain threshold sizes in magnetite. *Journal of Geophysical Research, Solid Earth* 78(11):1780–1793.
28. Kasama T (2006) Magnetic properties, microstructure, composition, and morphology of greigite nanocrystals in magnetotactic bacteria from electron holography and tomography. *American Mineralogist* 91(8-9):1216–1229.
29. Muxworthy AR, Williams W (2015) Critical single-domain grain sizes in elongated iron particles: implications for meteoritic and lunar magnetism. *Geophysical Journal International* 202(1):578–583.
30. Lindholm D (1984) Three-dimensional magnetostatic fields from point-matched integral equations with linearly varying scalar sources. *IEEE Transactions on Magnetics* 20:2025–2032.
31. Brown Jr. WF (1963) Micromagnetics. (Interscience Publishers).
32. Heider F, Dunlop DJ, Sugiura N (1987) Magnetic properties of hydrothermally recrystallized magnetite crystals. *Science (ISSN 0036-8075)* 236:1287–1290.
33. Tauxe L (2010) *Essentials of Paleomagnetism*. (Univ of California Press).